Northumbria Research Link

www.northumbria.ac.uk/nrl

northumbria
UNIVERSITY NEWCASTLE

Exploring Local Regularities for 3D Object Recognition

TIAN Huaiwen[1] and QIN Shengfeng[2, *]

1 *College of Mechanical Engineering, Southwest Jiaotong University, Chengdu 610031, China*
2 *Department of Design, Northumbria University, Newcastle upon Type, NE1 8ST*

Abstract: In order to find better simplicity measurements for 3D object recognition, a new set of local regularities is developed and tested in a stepwise 3D reconstruction method, including localized minimizing standard deviation of angles(L-MSDA), localized minimizing standard deviation of segment magnitudes(L-MSDSM), localized minimum standard deviation of areas of child faces (L-MSDAF), localized minimum sum of segment magnitudes of common edges (L-MSSM), and localized minimum sum of areas of child face (L-MSAF). Based on their effectiveness measurements in terms of form and size distortions, it is found that when two local regularities: L-MSDA and L-MSDSM are combined together, they can produce better performance. In addition, the best weightings for them to work together are identified as 10% for L-MSDSM and 90% for L-MSDA. The test results show that the combined usage of L-MSDA and L-MSDSM with identified weightings has a potential to be applied in other optimization based 3D recognition methods to improve their efficacy and robustness.

1 Introduction

Toward a future manufacturing environment underpinned by Industry 4.0 technologies, object recognition is a precursor to many other important robotic tasks, including grasping, manipulation, inspection and assembly.

3D object recognition from a 2D line drawing is a research topic related to machine intelligence and computer vision[1–2] and sketch-based interface and modeling[3].

A line drawing can be converted from freehand sketches involving sketch tidy-up processing[4–5]. It can also be derived from image segmentation or edge detection[6]. Another source for line drawing is from CAD packages such as AutoCAD®.

Popular methods of 3D object recognition from 2D line drawing are optimization based inflation methods. Most of them assume that the face topology of a line drawing is known in advance.

In general, optimization-based inflation methods iteratively change depths to vertices and test interim results with a set of compliance functions involving various regularities. These methods treat the 3D object recognition from a 2D line drawing as a global optimization problem involving a large number of variables and a good number of image regularities with different weightings. Thus, the main problem with these methods is that they are computationally heavy and with no guarantee for a good result when dealing with a complex drawing. In addition, various regularities are applied globally and guides for setting up weightings for regularity are unclear due to the lack of knowledge about their relative importance.

The strategic solution to the problem has twofold. First, adopt a divide-and-conquer strategy to divide a whole task into multiple smaller and easy-to-solve ones at local level. Second, use most influential local regularities with effective weightings to reduce the problem complexity in optimization.

In Ref. [7], a divide-and-conquer strategy is applied to decompose a complex line drawing into component drawings or simpler ones and each simpler drawing can be recognized easily and locally. In Ref. [8], a level-by-level 3D reconstruction method is explored to divide a global optimization-based 3D reconstruction from a complex drawing into multiple local reconstructions from a subset of the drawing, based on its face/surface connection graph.

However, there is very little work on the development of local regularities and identification of their usages in terms of what regularities should be used together and how to set up their weightings.

In this paper, a stepwise 3D reconstruction method is used for exploring local regularities for recognizing a 3D polyhedral object from its 2D axonometric drawing. As a result, it is found that two local regularities: L-MSDA and L-MSDSM need to be used together as a combined regularity and their weightings are 10% for L-MSDSM and 90% for L-MSDA respectively. This combined local regularity has a potential to be applied in various optimization-based inflation methods in order to have

---

* Corresponding author. E-mail: sheng-feng.qin@northumbria.ac.uk

better efficacy and robustness. A prototype platform on Matlab® has been developed for case studies and evaluation. The evaluation results demonstrate that the proposed method is a good way to explore various regularities for objects with resolvable representations[9]. The contributions of this paper include:

(1) Exploration and development of the localized regularities: L-MSDA, L-MSDSM, L-MSDAF, L-MSSM and L-MSAF and the development of a method to study their relative importance;

(2) Identification of the usage for combining L-MSDA and L-MSDSM together;

(3) Test cases from AutoCAD drawings.

The paper structure is as the following. The related work and the utilized stepwise reconstruction method are presented in sections 2 and 3 respectively. In section 4, the exploration and identification of key local regularities and their usages are followed up before case evaluations in section 5. Finally, conclusions are drawn in section 6.

2   Related work

Early work on 3D recognition of an object from a line drawing is focused on line labelling[10–11], attempting to evaluate whether the drawing represents a valid solid object. An optimization-based inflation process has been then developed to reconstruct 3D objects.

MARILL[12] observed that human minds prefer a simple interpretation over a complex one. But, how to measure the simplicity of a recognized object is not clearly and well defined. In Ref. [12], the simplicity is measured by minimizing the differences among angles created between lines at junctions across the reconstructed object. It is termed as the minimizing the standard deviation of angles (MSDA). LECLERE and FISCHLER[13] added face planarity, and LIPSON and SHPITALNI[14] added more image regularities into an optimization process, and demonstrated the ability to recognize a wide range of objects. ERIC and BROWN[15] replaced the MSDA with minimizing the standard deviation of segment magnitudes (MSDSM) and produced better results for some cases compared with MSDA. This research suggested searching for alternative regularities to reflect the simplicity measurement, which inspired our work here.

VARLEY and MARTIN[16] found that the cubic corner property was particularly useful. A cubic corner is a junction where three mutually orthogonal planes meet, which can is derived and understood from MSDA. The relationship between a cubic corner in 3D and its 2D projection was established by PERKINS[17].

YONG and FANG[18] studied a direct 3D recognition method from a 2D drawing, requiring two sets of information from the drawing: a list of faces and a cubic corner. This research demonstrated that the use of face connections to trace down a reconstruction process could be an effective and accurate way to solve a 3D reconstruction problem.

For reducing the complexity of a 3D reconstruction, LIU, et al[19], considered MSDA and face planarity as two most important constraints. SUN, et al[20], reviewed the usages of various regularities in literature and recommended a set of key regularities for general 3D reconstruction based on the automatic relevance determination method. It is believed that the regularities are not equally informative in the simplicity measuring and some may deal with mainly to noise.

It is clear that many regularities have been used in previous research but their relative relationships are not known. This study demonstrates a way of studying their relationships or relative importance, exploring possible regularities further and identifying their usages.

3   Stepwise 3D reconstruction Method

3.1   Principles of the stepwise 3D reconstruction method

An engineering object can be represented by an isometric drawing or oblique drawing with or without hidden lines (Fig. 1). The understanding of a 2D drawing into a 3D object can be a component-based method grounded on a theory of human image understanding[21] or a global optimization based method[13]. Interpreting a 3D object from a oblique drawing can be found in[22–24] .
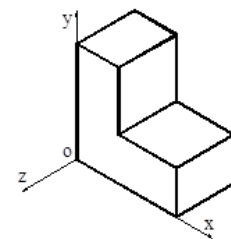
(a) Isometric drawing
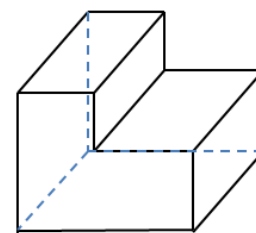
(b) Oblique drawing

Fig. 1.   Axonometric projection

A component based method solves a problem in a stepwise fashion and might be quick and reliable because it finds solutions step-by-step and at each step, the problem is less complicated for solving. Thus, in this study we utilized a stepwise 3D reconstruction method.

This stepwise 3D reconstruction method is based on the theory of axonometric projection. Under an axonometric projection, a 3D point (X, Y, Z) will produce a 2D

projection point (x, y). Their relation is

$$\begin{bmatrix} x & y & 0 & 1 \end{bmatrix} = \begin{bmatrix} X & Y & Z & 1 \end{bmatrix} \cdot T, \qquad (1)$$

where

$$T = T_1 T_2 T_3 = \begin{bmatrix} \cos\alpha & \sin\alpha\sin\beta & 0 & 0 \\ 0 & \cos\beta & 0 & 0 \\ \sin\alpha & -\cos\alpha\sin\beta & 0 & 0 \\ 0 & 0 & 0 & 1 \end{bmatrix}, \qquad (2)$$

T_1 and T_2 represent two rotation transformation matrices while T_3 describes an orthographic projection. Under this transformation in Eq. (1), every 3D vertex $V(X, Y, Z, 1)$ in the 3D object has a corresponding 2D point in the drawing represented as a vertex $v(x, y, 0, 1)$ from $v = VT$.

T is not reversible. But when a constraint is introduced in each step, in a stepwise reconstruction process, saying that a point to be reconstructed is on a planar face (face regularity is applied explicitly here), T is then converted into a reversible matrix and it can be used to support 3D reconstruction by a reverse transformation.

In generality, a planar face in 3D can be represented by Eq. (3), where (a, b, c) is the face normal and d is the distance to the origin:

$$aX + bY + cZ + d = 0. \qquad (3)$$

Now, if this face is used as the constraint, T matrix can be updated as a reversible matrix R.

$$R = \begin{bmatrix} \cos\alpha & \sin\alpha\sin\beta & a & 0 \\ 0 & \cos\beta & b & 0 \\ \sin\alpha & -\cos\alpha\sin\beta & c & 0 \\ 0 & 0 & d & 1 \end{bmatrix}. \qquad (4)$$

With R, for any known 2D point (x, y) on the drawing, its corresponding 3D point V can be obtained by Eq. (5), that is

$$V = vR'. \qquad (5)$$

3.2 Stepwise 3D reconstruction scheme with local optimization

Based on the above ideas, our stepwise 3D reconstruction method was scheduled in the following steps:

Step 1: Find faces[25–29] in the drawing and establish a face connection graph based on a resolvable representation[9] during the data preparation process. In a connection graph, a parent face connects to each child face via a connecting edge. Fig. 2(a) shows faces of an exemplar drawing and Fig. 2(b) gives its face connection graph. For example, connecting edges e_1 and e_2 with the parent face F_1 have two child faces F_2 and F_3 respectively.
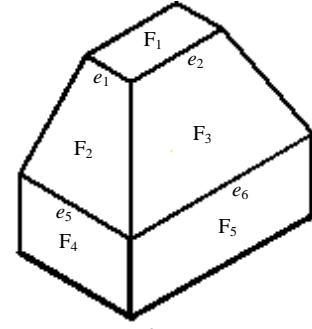
(a) Faces within a 2D drawing
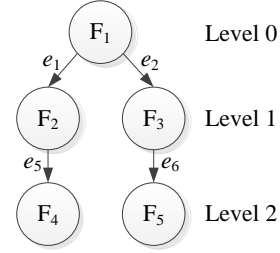
(b) Face connection graph (FCG)

Fig. 2. Faces in a 2D drawing and their connection graph

Step 2: Set the first reference face (the parent face) for 3D reconstruction. The first face is selected from the root face in the FCG connection graph. Normally, it is parallel to one of datum planes and its orientation can be interactively specified so that the normal information regarding to parameters: a, b and c for the reference plane equation can be obtained and the fourth parameter d can be computed for Eq. (4). Let the face pass through the origin(d=0) and its normal vector (a, b, c) will be easily decided as (1, 0, 0), or (0, 1, 0), or (0, 0, 1). For a given isometric projection, It is known that the project transformation parameters such as: α=45° and β=35.26° as used in AutoCAD and thus R can be formed from Eq. (4). This enables all vertices on the reference face to be reconstructed.

Step 3: Reconstruct its child faces level-by-level (or step-by-step). Once a parent face is known in 3D and its connecting edges are known in 3D too. Their connections to child faces can be traced from the face connection graph. When reconstructing child faces, a local optimization-based strategy is applied for reducing the complexity of global optimization and having better efficacy. At each step, rotating the parent face in 3D about one of its 3D connecting edges, new possible child faces with proper connections to each other can be obtained. Therefore, after each rotation, local regularities in Eq. (11) (detailed in section 4) can be evaluated, and if the regularities are not met, the process will continue to search for a new rotation angle until a satisfied solution is found so that local regularities are met.

Step 4: Move to the next level on the face connection graph and repeat Step 3 until all faces are reconstructed.

Next section details how to explore best regularities and

their usages for local optimization in our study.

4 Establishment of local regularities for local optimization

4.1 Searching localized regularities for optimization

The face planarity was explicitly used in our study because face connections was used in the face reconstruction.

We first explored the following localized regularities: L-MSDA, L-MSDSM, localized minimum standard deviation of areas of child faces(L-MSDAF), localized minimum sum of segment magnitudes of common edges (L-MSSM), and localized minimum sum of areas of child face(L-MSAF). They are described as follows.

4.1.1 Localized MSDA regularity(L-MSDA)

MSDA[12] is regarded as a global regularity[30]. Based on the concept of MSDA, we developed a localized MSDA (L-MSDA) regularity, that is, all evaluable angles at the current reconstruction level must be similar or with the minimum standard deviation.
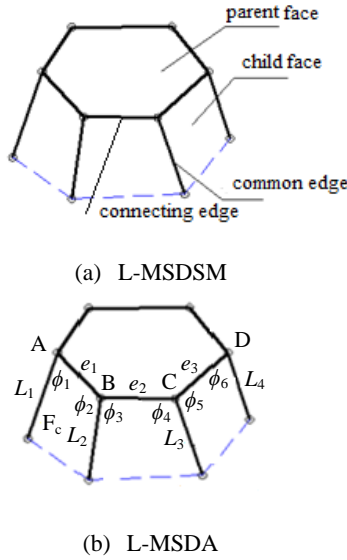

(a) L-MSDSM

(b) L-MSDA

Fig. 3 Localized MSDA and MSDSM

At the current level as shown in Fig. 3(b), the parent face P has three child faces connected to edges AB, BC and CD. The corresponding edge lengths are e_1, e_2 and e_3. There are four vertices A, B, C and D connecting with unknown angles ϕ_1 to ϕ_6 and unknown edge segments L_1 to L_4. Therefore, six angles ϕ_1 to ϕ_6 and four line segments L_1 to L_4 on child faces are evaluable at the current level. While rotating the child face F_c, all these unknown variables change.

For generality, suppose there are k vertices forming $(k–1)$ edges which are linked to child faces. The known angles at k vertices are β_i (i=1, 2, …, k). The $(k–1)$ edges have known edge lengths e_j (j=1, 2, …, $k–1$). For unknown variables, there are N angles ϕ_u (u=1, 2, …, N) and M line segments L_v (v=1, 2, …, M).

The localized standard deviation of (evaluable) angles is given by

$$\delta = \sqrt{\frac{1}{N}\sum_{u=1}^{N}(\varphi_u - \varphi_m)^2} \, , \qquad (6)$$

where ϕ_m is the average of the angles, i.e., $\sum_{u=1}^{N}\phi_u / N$.

4.1.2 Localized MSDSM regularity(L-MSDSMA)

Similarly, we adapted the concept of the global regularity MSDSM as in Ref. [15], and developed a localized one: L-MSDSM, that is, all edges meeting at junctions associated with the parent faces must be similar or with the minimum standard deviation.
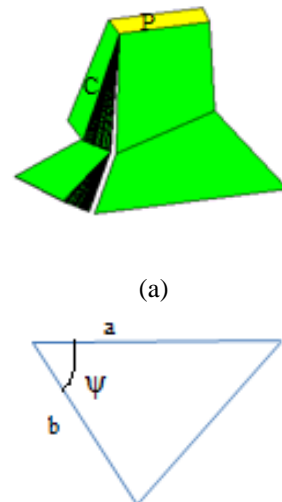
At current reconstruction level, only the common edges are taken into consideration. That is, if there exist M common edges, as shown in Fig. 3(a), the standard deviation of segment magnitudes is represented as

$$\sigma = \sqrt{\frac{1}{M}\sum_{v=1}^{M}(L_v - L_m)^2} \, , \qquad (7)$$

where L_v is the length of the vth common edge, and L_m is the average length of all common edges, i.e., $\sum_{v=1}^{M}L_v / M$.

4.1.3 Localized minimum standard deviation of areas of child faces (L-MSDAF)

Fig. 4(a) demonstrates multiple candidates for a child face C associated to its parent face P. Inspired from the regularities such as MSDA and MSDSM, and knowing that a triangle area is related to the triangle's two adjacent edges and their interior angle, in terms of $a \cdot b \cdot \sin(\psi)$, as shown in Fig. 4(b), we developed the minimum standard deviation of areas of child faces as a regularity and hoped it could have a coupled effect of MSDA and MSDSM.

(a)

Let the parent face P has G child faces to be reconstructed at current level.   The areas of child faces are A_i (i=1,…,G), the standard deviation of areas of child faces ξ is:

$$\xi = \sqrt{\frac{1}{G}\sum_{i=1}^{G}(A_i - A_m)^2} \ , \qquad (8)$$

where A_m is the average area of all connected child faces, i.e., $\sum_{i=1}^{G} A_i / G$.

4.1.4   *Localized minimum sum of segment magnitudes of common edges (L-MSSM)*

As a general principle, humans tend to interpret a 3D object as simple or compact as possible from a 2D image. From this principle, we designed another local regularity attempting to make the reconstructed object simple. It is the minimum sum of segment magnitudes of common edges (L-MSSM).

$$Min \sum_{v=1}^{M} L_v \ , \qquad (9)$$

4.1.5   *Localized minimum sum of areas of child face (L-MSAF)*

Similar to L-MSSM, we developed the minimum sum of areas of child faces. The localized minimum sum of areas of child face (L-MSAF) is represented as

$$Min \sum_{i=1}^{G} A_i \ . \qquad (10)$$

4.2   Evaluating effectiveness of regularities

After developing the five localized regularities, in order to identify key regularities, we conducted an effectiveness evaluation.

A non-regular pentagonal prism and its variations were used in our tests. The test prism is shown in Fig. 5 and its height is 70.   Nine variations were created by keeping its top section and the height unchanged meanwhile scaling the bottom section about its center with scaling factors (SF= 3, 2.5, 2, 1.5, 1, 0.8, 0.5, 0.3 and 0.1 respectively). Some variations are shown in Fig. 6.
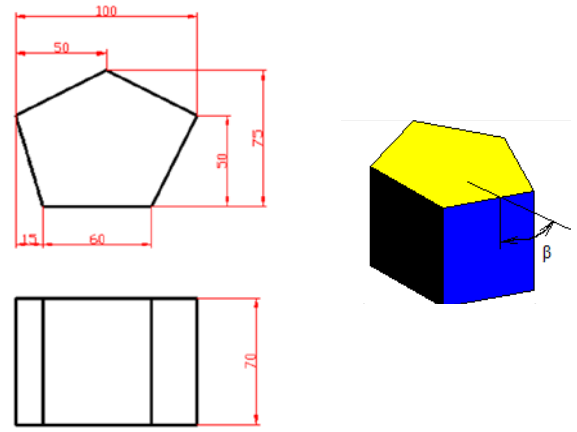

Fig. 5 test prism

SF=3   SF=2.5   SF=1.5   SF=1.2

SF=0.8   SF=0.5   SF=0.3   SF=0.1
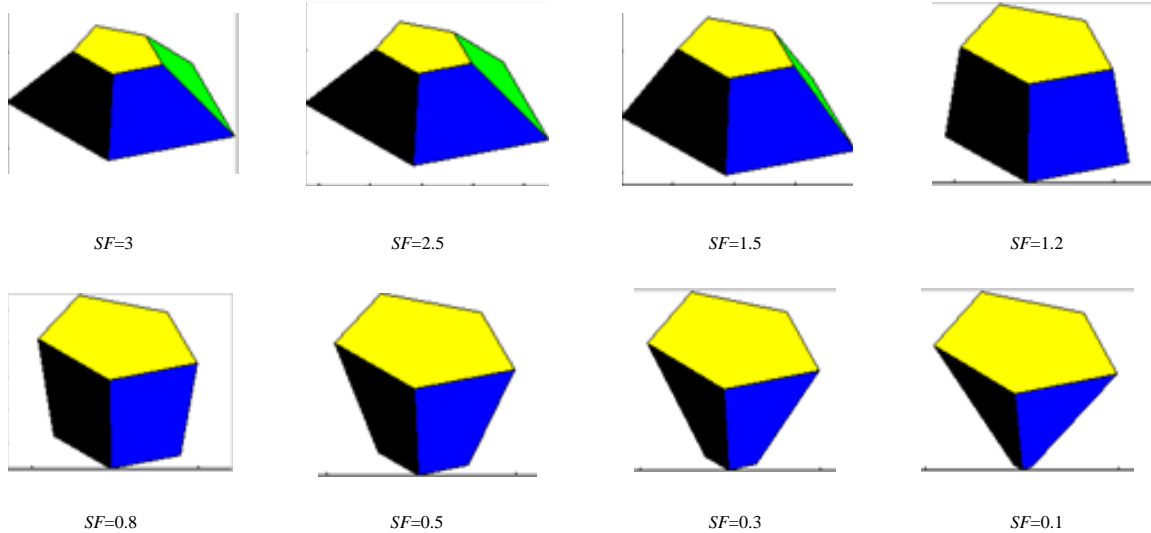
Fig. 6.   variations of the original prism for testing

During the test, for each case, we used the top face as the parent face to construct its child faces.   During a reconstructing, the parent face was rotated about a connecting edge and its child faces were then constructed and evaluated with single regularity.   Note that the child faces were sharing a common edge between two of them, therefore, all child faces were constructed in one go after each rotation.

After receiving a reconstructed result, the effectiveness of the corresponding regularity was examined to see how the reconstructed was close to the original one. The effectiveness was measured by two factors: form and size distortions. The former was calculated as a relative angle error $\Delta\beta$. For each test case, the ground truth value of the angle β, as shown in Fig. 5, was known, giving $\Delta\beta = abs\ (\alpha - \beta)/\beta$ as a measure. The latter was similarly calculated as a relative area error Δa between the true surface area(a_0) and the reconstructed surface area(a_c), that is, $\Delta a = abs\ (a_c - a_0)/a_0$. The test results are shown in Table 1.

Table 1. Effectiveness test results of the designated regularities

| Operation index	Test Cases		Ground True values		L-MSDSM		L-MSDA		L-MSDAF		L-MSSM		L-MSAF	
			Angle β	Area a_0	Angle α	Area a_c	angle α	Area a_c	angle α	Area a_c	angle α	Area a_c	angle α	Area a_c
1	SF=3.0	Calculated	49	57369	45	55623	82	80394	46	56047	19	46636	5	43527
		errors/%			–8	-3	67	40	-6	-2	-61	-18	-90	-24
2	SF=2.5	Calculated	57	43961	54	42753	79	56338	55	43147	25	34025	10	31760
		errors/%			–5	-3	39	28	-4	-2	-56	-23	-82	-28
3	SF=2	Calculated	67	33465	64	32344	77	38002	67	33465	34	24774	16	23061
		errors/%			-4	-3	15	14	0	0	-49	-26	-76	-31
4	SF=1.5	Calculated	78	25403	77	25047	80	26156	80	26156	48	18740	27	17446
		errors/%			-1	-1	2	3	2	3	-38	-26	-65	-31
5	SF=1.2	Calculated	85	21645	85	21645	85	21645	86	21999	57	16116	37	15170
		errors/%			0	0	0	0	1	2	-33	-26	-56	-30
6	SF=1	Calculated	90	19595	3	18160	90	19595	82	17379	64	14752	43	13926
		errors/%			-97	-7	0	0	-9	-11	-29	-25	-52	-29
7	SF=0.8	Calculated	95	17771	95	17771	96	18114	86	15467	70	13468	50	12814
		errors/%			0	0	1	2	-9	-13	-26	-24	-47	-28
8	SF=0.5	Calculated	102	15191	103	15520	105	16262	99	14349	80	11790	60	11260
		errors/%			1	2	3	7	-3	-6	-22	-22	-41	-26
9	SF=0.3	Calculated	107	13708	108	14042	110	14817	105	13129	87	10710	66	10213
		errors/%			1	2	3	8	-2	-4	-19	-22	-38	-25
10	SF=0.1	Calculated	111	11951	112	12265	116	13985	111	11951	93	9519.7	72	9098.2
		errors/%			1	3	5	17	0	0	-16	-20	-35	-24
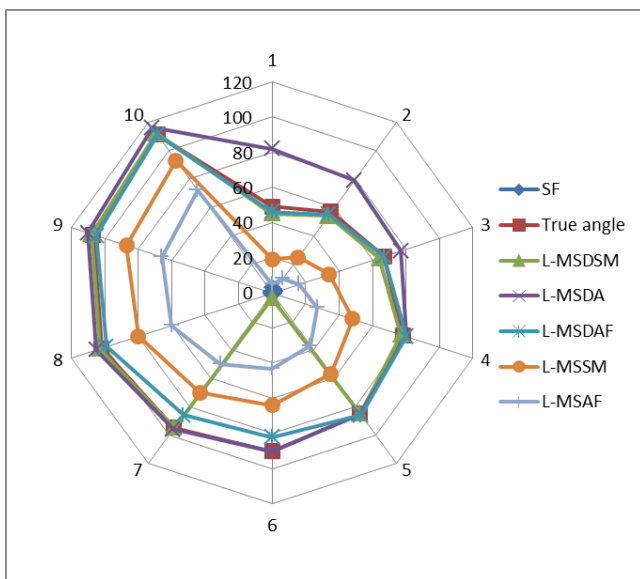
Fig. 7.   Radar chart of the form distorsions

The relationship between the ground true angles and corresponding reconstructed angles for each regularity is shown in Fig. 7 as a Radar chart. From Fig. 7, the following points are clearly indicated. First, two regularities of L-MSSM and L-MSAF always produce a big angular (or form) distortion, thus, they are not good enough to be a candidate as a key regularity. For L-MSDAF, its angular errors are negative for most of cases and worst around 90 degrees, thus, it is still not an ideal choice. Now looking at L-MSDA and L-MSDSM, for some cases they are similar and quite close to the true value, and for the others, their errors are complemented to each other, i.e., when L-MSDSM produces positive errors such as for index 6 and index 1, L-MSDA produces negative errors for the same cases. This phenomenon is also observed from the area errors in Fig 8. This suggests that it would be better to use both of them as a combination.
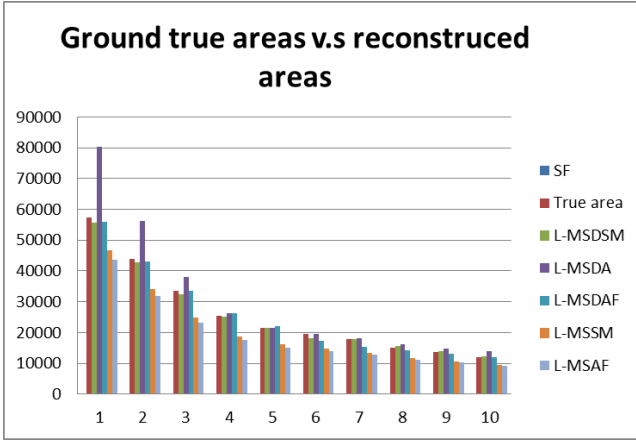
Fig. 8. Ground true areas against reconstructed areas

4.3 Identifying weights for establishing the local regularities

4.3 Identifying weights for establishing the local regularities

From the above observations, we decided to test a combined regularity:

$$\tau = a \cdot \mathrm{Min}(\sigma) + b \cdot \mathrm{Min}(\delta), \qquad (11)$$

a and b are weightings for L-MSDSM and L-MSDA respectively. We constrained the weightings a and b with $a+b=1$ and a, $b>0$.

In order to identify weightings for the combined usage of L-MSDA and L-MSDSM, different weighting schemes were tested as a varying from 0%, 10%, ..., to 100%. The test results are shown in Table 2.

Table 2.   Form distortions against different weighting schemes

| | | True Angle | weighting a | | | | | | | | | | |
		β	0%	10%	20%	30%	40%	50%	60%	70%	80%	90%	100%
SF=3.0	Calculated	49	82	49	47	46	46	45	45	45	45	45	45
	errors/%		67	0	−4	−6	−6	−8	-8	-8	-8	-8	-8
SF=2.5	Calculated	57	79	57	55	55	54	54	54	54	54	54	54
	errors/%		38.6	0	-3.5	-3.5	-5	-5	-5	-5	-5	-5	-5
SF=2	Calculated	67	77	67	66	65	65	65	65	65	65	64	64
	errors/%		15	0	-1.5	-3	-3	-3	-3	-3	-3	-4.5	-4.5
SF=1.5	Calculated	78	80	78	77	77	77	77	77	77	77	77	77
	errors/%		2.6	0	-1.3	-1.3	-1.3	-1.3	-1.3	-1.3	-1.3	-1.3	-1.3
SF=1.2	Calculated	85	85	85	85	85	85	85	85	85	85	85	85
	errors/%		0	0	0	0	0	0	0	0	0	0	0
SF=1	Calculated	90	90	90	90	90	90	90	90	90	90	90	3
	errors/%		0	0	0	0	0	0	0	0	0	0	-97
SF=0.8	Calculated	95	96	95	95	95	95	95	95	95	95	95	95
	errors/%		1	0	0	0	0	0	0	0	0	0	0
SF=0.5	Calculated	102	105	103	103	103	103	103	103	103	103	103	103
	errors/%		3	1	1	1	1	1	1	1	1	1	1
SF=0.3	Calculated	107	110	108	108	108	108	108	108	108	108	108	108
	errors/%		3	1	1	1	1	1	1	1	1	1	1
SF=0.1	Calculated	111	116	113	113	112	112	112	112	112	112	112	112
	errors/%		4.5	2	2	1	1	1	1	1	1	1	1

From Table 2, it is clear that the weighting scheme 10% L-MSDSM+90% L-MSDA gives the minimum form errors for all cases but the last one. Therefore, we established Eq. (12) as our key combined regularity with determined weightings and applied it in our reconstruction strategy for local optimization.

$$\mathrm{Min}\ \tau ' = 0.1\,\mathrm{Min}(\sigma) + 0.9\,\mathrm{Min}(\delta), \qquad (12)$$

5 Tests and result analysis

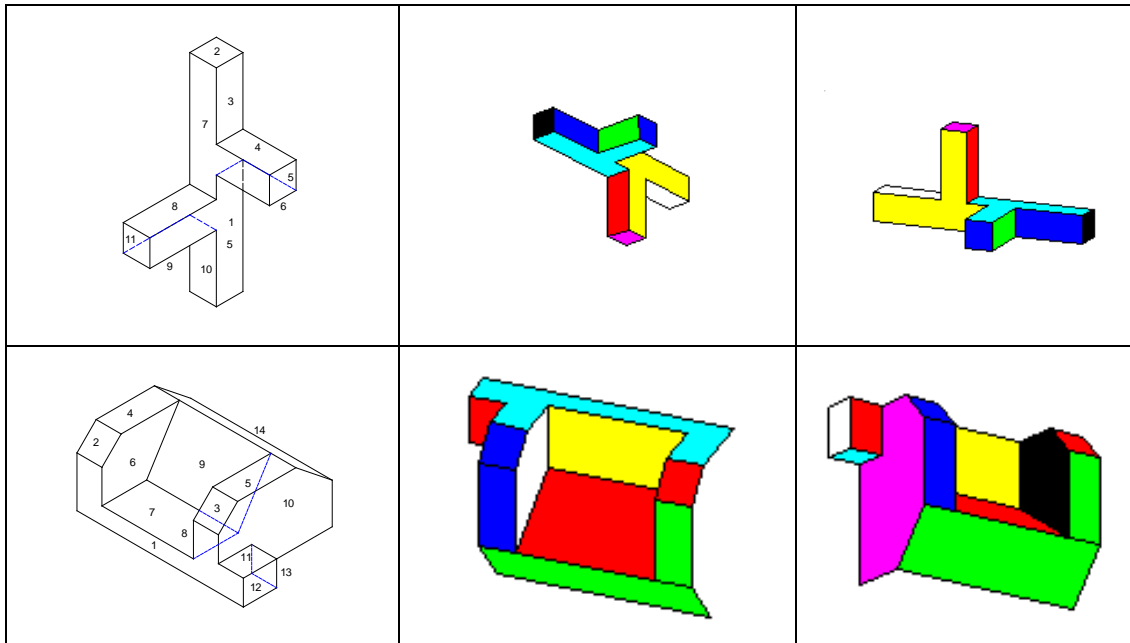Our stepwise reconstruction method has been prototyped with the identified local regularities in Matlab® for all our case studies. We used isometric 2D drawings from AutoCAD as input for 3D recognition. The parent face and the corresponding face connection graphs for each case were produced manually during a data preparation process.

5.1 Satisfactory cases

First, we tested our local and stepwise reconstruction method with different cases, as shown in Table 3. The first four cases(top four rows) show the input drawings with vertices and face indexes. The face F1 was chosen as the root face for each case. The other cases give face indexes only. Each reconstructed result is displayed in two columns with different viewpoints. All the reconstructed results are satisfactory.

Table 3. Examples of line drawings with analytical solutions

Input-2D drawings	Reconstructed result	Another view

5.2 Challenging/failed cases

During our tests, we met some challenging cases. In general, if an object does not have solvable sequences as discussed in[9] such as Sugihara torus, as is shown in Fig. 9, our method will fail to solve its reconstruction problem.
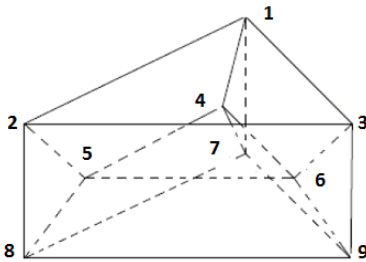

Fig. 9 Sugihara torus

6 Conclusions

(1) The proposed stepwise 3D reconstruction method with local regularities can recognize polyhedral objects with resolvable presentations, and it provides a way to decompose a complex reconstruction problem into simpler local optimization problems.

(2) Two localized regularities namely localized MSDA (L-MSDA) and localized MSDSM(L-MSDSM) need to be utilized together and best weightings for their usage are 10% L-MSDSM and 90% L-MSDA.

(3) The combined local regularity can be adopted in other divide-and-conquer reconstruction methods.

(4) In the future, the comparison study between local regularity-based solution and global regularity-based solution will be carried out to test their performance and suitability.

References

[1] YANG L J, LIU J Z, TANG X O. Complex 3D general object reconstruction from line drawings[C]//*IEEE international conference on computer vision (ICCV)*, Sydney, Australia, Dec 1–8, 2013: 1433–1440.

[2] ZOU C Q, YANG H, LIU J Z. Separation of line drawings based on split faces for 3D object reconstruction[C]//*IEEE Conference on Computer Vision and Pattern Recognition*, Columbus, OH, USA, Jun 23–28 , 2014: 692–699.

[3] ZHANG J, WANG Y, TANG Z. Recovering solid geometric object from single line drawing image[J]. *Multimedia Tools and Application*, 2015, DOI: DOI 10.1007/s11042-015-2966-x.

[4] QIN S F, WRIGHT D K, JORDANOY I N. On-line segmentation of freehand sketches by knowledge-based nonlinear thresholding operations[J]. *Pattern Recognition*, 2001, 34(10): 1885–1893.

[5] WANG S, QIN S, GAO M. New grouping and fitting methods for interactive overtraced sketches[J]. *Visual Computer International Journal of Computer Graphics*, 2014, 30(3): 285–297.

[6] MAINI R, AGGARWAL H. Study and comparison of various image edge detection techniques[J]. *International Journal of Image Processing*, 2009, 3(1): 1–11.

[7] LIU J, CHEN Y X. TANG X. Decomposition of complex line drawings with hidden lines for 3d planar-faced manifold object reconstruction [J]. *IEEE T-PAMI*, 2011, 33(1): 3–15.

[8] QIN S, TIAN H W. On the algorithm for reconstruction of polyhedral objects from a single line drawing[C]//*International Conference on Automation and Computing, IEEE*, 2015.

[9] SUGIHARA K. Resolvable representations of polyhedral[J]. *Discrete and Computational Geometry*, 1999, 21(2): 243–255.

[10] CLOWES M B. On seeing things[J]. *Artificial Intelligence*, 1971, 2(1): 79–116.

[11] KANADE T. A theory of Origami world[J]. *Artificial Intelligence*, 1980, 13(3): 279–311.

[12] MARILL T. Emulating the human interpretation of line-drawings as three-dimensional objects[J]. *International Journal of Computer Vision*, 1991, 6(2): 147–161.

[13] LECLERC Y G, FISCHLER M A. An optimization-based approach to the interpretation of single line drawings as 3D wire frames[J]. *International Journal of Computer Vision*, 1992, 9(2): 113–136.

[14] LIPSON H, SHPITALNI M. Optimization-based reconstruction of a 3D object from a single freehand line drawing[J]. *Computer-Aided Design*, 2012, 28(8): 651–663.

[15] BROWN E W. Why we see three-dimensional objects: another approach[R]. Internal Report: *Northeastern University*, 1994. *http://citeseerx.ist.psu.edu/viewdoc/download?doi=10.1.1.71.3308&*

rep=rep1&type=pdf, Access on March 1, 2014.

[16] VARLEY P A C, MARTIN R R. The junction catalogue for labelling line drawings of polyhedra with tetrahedral vertices[J]. *International Journal of Shape Modeling*, 2011, 07(1):23-44.

[17] PERKINS D N. Cubic corners, oblique views of pictures, the perception of line drawings of simple space form, geometry and the perception of pictures: three studies [R], 1968, Harvard University, Reprinted in Harvard Project Zero Technical Rep. No. 5, 1971, http://files.eric.ed.gov/fulltext/ED114328.pdf, accessed on May 23, 2014.

[18] YONG T L, FANG F. 3D reconstruction of polyhedral objects from single parallel projections using cubic corner[J]. *Computer-Aided Design*, 2011, 43(8): 1025–1034.

[19] LIU J Z, CAO L L, LI Z G, et al. Plane-based optimization for 3D object reconstruction from single line drawings[J]. *IEEE Transactions on Pattern Analysis and Machine Intelligence*, 2008, 30(2): 315–327.

[20] SUN Y, LEE Y T, SUN J. Regularity selection for effective 3D object reconstruction from a single line drawing[J]. *Pattern Recognition Letters*, 2008, 29(10): 1486–1495.

[21] BIEDEMAN I. Recognition-by-components: a theory of human image understanding[J]. *Psychological Review*, 1987, 94(2): 115–147.

[22] QIN S F, WRIGHT D K, JORDANOV I N. From on-line sketching to 2D and 3D geometry: a system based on fuzzy knowledge[J]. *Computer-Aided Design*, 2000, 32(00): 851–866.

[23] LAMB D, BANDOPADHAY A. Interpreting a 3D object from a rough 2D line drawing[C]//*Proceedings of the 1st conference on Visualization '90,* San Francisco, *Oct 23-26,* 1990: 59–66.

[24] COMPANY P, CONESA J, ALEIXOS N. Axonometric Inflation in Line Drawings Reconstruction[R], 2001, Jaume I University, http://www.regeo.uji.es/publicaciones/regeo01.pdf. Accessed on Mar 1, 2014.

[25] LIU J, LEE Y T. A Graph-Based Method for Face Identification from a Single 2D Line Drawing[J]. *IEEE Transactions on Pattern Analysis & Machine Intelligence*, 2001, 23(10): 1106–1119.

[26] LIU J, LEE Y T, CHAM W K. Identifying faces in a 2D line drawing representing a manifold object[J]. *IEEE Transactions on Pattern Analysis and Machine Intelligence*, 2002, 24(12): 1579–1593.

[27] VARLEY P A C, COMPANY P. A new algorithm for finding faces in wireframes[J]. *Computer-Aided Design*, 2010, 42(4): 279–309.

[28] LEONG M C, LEE Y T, FANG F. A Search-and-Validate Method for Face Identification from Single Line Drawings[J]. *IEEE Transaction on Pattern Analysis and Machine Intelligence*, 2013, 35(11): 2576–2591.

[29] FANG F, YONG T L. Efficient decomposition of line drawings of connected manifolds without face identification[J]. *Computer-Aided Design*, 2014, 51(6): 18–30.

[30] VARLEY P A C, MARTIN R R. Estimating depth from line drawings[C]//*Proceedings of the seventh ACM symposium on Solid modeling and applications*, Saarbrücken, Germany, Jun 17–21, 2002: 180–191.

Biographical notes

TIAN Huaiwen, born in 1965, is a arofessor at *School of Mechanical Engineering, Southwest Jiaotong University, China*. His main research interests include computer graphics, CAD, and reverse engineering.

QIN Shengfeng, born in 1962, is a arofessor at *School of Design, Northumbria University, UK*. His main reserach interests include sketch-based interface and modeling, digital design and manufacturing tools.